9358 *Inorg. Chem.* **2010**, *49*, 9358–9368
DOI: 10.1021/ic101038z

Inorganic Chemistry
Article

Cyanocarbanion-Based Spin-Crossover Materials: Photocrystallographic and Photomagnetic Studies of a New Iron(II) Neutral Chain

Gaelle Dupouy,[†] Smail Triki,[*,†] Mathieu Marchivie,[†,‡] Nathalie Cosquer,[†] Carlos J. Gómez-García,[§] Sébastien Pillet,[⊥] El-Eulmi Bendeif,[⊥] Claude Lecomte,[⊥] Saket Asthana,[¶] and Jean-François Létard[¶]

[†]*Université Européenne de Bretagne (ueb), Université de Brest, UMR CNRS 6521, 6 Avenue V. Le Gorgeu, C.S. 93837, 29238 Brest, France,* [§]*Instituto de Ciencia Molecular, Universidad de Valencia, 46980 Paterna, Valencia, Spain,* [⊥]*CRM2, UMR CNRS 7036, Institut J. Barriol, Nancy-Université, BP239, 54506 Vandoeuvre les Nancy, France, and* [¶]*CNRS, Université Bordeaux, ICMCB, 87 Av. Doc. A. Schweitzer, F-33608 Pessac, France.* [‡]*Present address: EA 4138, Université de Bordeaux, 146 rue Léo Saignat, 33076 Bordeaux, France.*

Received May 22, 2010

A new iron(II) chain of formula $[Fe(abpt)_2(tcpd)]$ [**1**; $(tcpd)^{2-} = [C_{10}N_6]^{2-} = (C[C(CN)_2]_3)^{2-}$ = 2-dicyanomethylene-1,1,3,3-tetracyanopropanediide anion, abpt = 4-amino-3,5-bis(pyridin-2-yl)-1,2,4-triazole] has been synthesized and characterized by IR spectroscopy, detailed variable-temperature single-crystal X-ray diffraction, magnetic and photomagnetic measurements. The crystal structure determination of **1** reveals a one-dimensional structural architecture in which the $(tcpd)^{2-}$ cyanocarbanion acts as a μ_2-bridging ligand and the two abpt molecules act as chelating ligands. Detailed X-ray diffraction studies as a function of the temperature (293−10 K) showed a strong modification of the iron coordination sphere, whose characteristics are in agreement with the presence of a spin-crossover transition from high spin (HS) to low spin (LS) in **1**. The average Fe−N distances at room temperature, at 10 K following a flash cooling, and at 10 K after subsequent HS-to-LS relaxation are in the range expected for 100%, 50%, and 25% fractions of HS Fe^{II}, respectively. These observations are consistent with the presence of ca. 25% residual HS species at low temperatures, as derived from the magnetic data. The signature of a photoinduced metastable HS state in **1** has been detected by performing coupled photomagnetic and photocrystallographic analyses. The limiting *T*(LIESST) value associated with the light-induced excited-spin-state trapping effect was derived as 35 K, in good agreement with the thermal dependence of the unit cell volume upon irradiation. Kinetic studies governing the photoinduced HS/LS process have been recorded at different temperatures; a reverse-LIESST effect has been evidenced at 10 K as a reduction of the residual HS fraction by irradiating the sample at 830 nm.

Introduction

Spin-crossover (SCO) complexes have been widely investigated over the last 30 years[1,2] and are still attracting intense research interest given the many possible applications of such complexes in the development of novel electronic devices, especially as molecular switches.[3,4] The electronic activity of the SCO complexes is inherent to the potential of some pseudo-octahedral transition-metal complexes to display a magnetic transition between the high-spin (HS) and low-spin (LS) states through external stimuli such as temperature, pressure, magnetic field, or light irradiation.[4−7] Such a SCO phenomenon occurs in the d^4−d^7 transition-metal complexes,[8−15] but the most studied examples to date are those based on Fe^{II} (the d^6 configuration), for which a

*To whom correspondence should be addressed. E-mail: smail.triki@univ-brest.fr.

(1) Gütlich, P., Goodwin, H. A., Eds. Spin Crossover in Transition Metal Compounds I−III. *Topics in Current Chemistry*; Springer Verlag: Berlin, 2004; Vols. *233*−*235*.
(2) Gamez, P.; Costa, J. S.; Quesada, M.; Aromí, G. *Dalton Trans.* **2009**, 7845–7853 and references cited therein.
(3) Létard, J.-F.; Guionneau, P.; Goux-Capes, L. *Top. Curr. Chem.* **2004**, *235*, 221–249.
(4) Cobo, S.; Molnár, G.; Real, J. A.; Bousseksou, A. *Angew. Chem., Int. Ed.* **2006**, *45*, 5786–5789.
(5) Decurtins, S.; Gütlich, P.; Köhler, C. P.; Spiering, H.; Hauser, A. *Chem. Phys. Lett.* **1984**, *105*, 1–4.
(6) Létard, J.-F. *J. Mater. Chem.* **2006**, *16*, 2550–2559.
(7) Niel, V.; Muñoz, M. C.; Gaspar, A. B.; Galet, A.; Levchenko, G.; Real, J. A. *Chem.—Eur. J.* **2002**, *8*, 2446–2453.
(8) Garcia, Y.; Gütlich, P. *Top. Curr. Chem.* **2004**, *234*, 49–62.
(9) Morgan, G. G.; Murnaghan, K. D.; Müller-Bunz, H.; McKee, V.; Harding, C. J. *Angew. Chem., Int. Ed.* **2006**, *45*, 7192–7195.
(10) Sim, P. G.; Sinn, E. *J. Am. Chem. Soc.* **1981**, *103*, 241–243.
(11) Halepoto, D. M.; Holt, D. G. L.; Larkworthy, L. F.; Leigh, G. L.; Povey, D. C.; Smith, G .W. *J. Chem. Soc., Chem. Commun.* **1989**, 1322–1323.
(12) van Konigsbruggen, P. J.; Maeda, Y.; Oshio, H. *Top. Curr. Chem.* **2004**, *233*, 259–324.
(13) Costes, J.-P.; Dahan, F.; Laurent, J.-P. *Inorg. Chem.* **1990**, *29*, 2448–2452.
(14) Ishikawa, R.; Matsumoto, K.; Onishi, K.; Kubo, T.; Fuyuhiro, A.; Hayami, S.; Inoue, K.; Kaizaki, S.; Kawata, S. *Chem. Lett.* **2009**, *38*, 620–621.
(15) Hayami, S.; Moriyama, R.; Shigeyoshi, Y.; Kawajiri, R.; Mitani, T.; Akita, M.; Inoue, K.; Maeda, Y. *Inorg. Chem.* **2005**, *44*, 7295–7297.

Published on Web 09/17/2010

Scheme 1. Some Examples of Cyanocarbanions

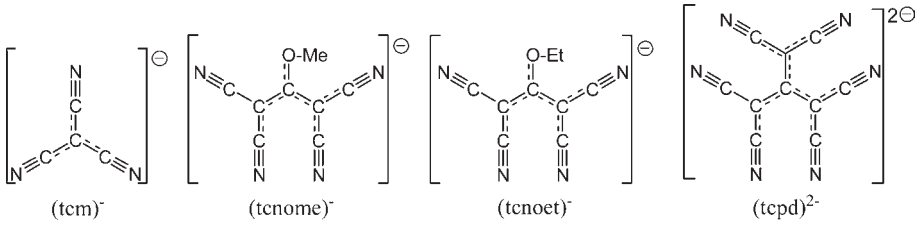

paramagnetic−diamagnetic transition from the HS ($S = 2$, $^5T_{2g}$) to LS ($S = 0$, $^1A_{1g}$) state is observed. In the past few years, numerous mononuclear compounds [mainly iron(II) complexes] have been extensively studied.[1,16−23] This was dictated by the necessity to understand the correlations between the intermolecular interactions (π-stacking, hydrogen-bonding, and van der Waals interactions between the metal active centers) and the desired SCO characteristics, such as thermal hysteresis related to cooperativity and light-induced excited-spin-state trapping (LIESST) effects. However, the lack of control of the noncovalent interactions in these discrete complexes hardens their supramolecular organization in the crystal. To better explore the cooperative effect between the active metal sites, Kahn et al.,[24−26] and others,[27−30] introduced an alternative approach based on the use of neutral suitable bridging ligands to covalently connect the metal centers. This strategy resulted in the synthesis of several iron(II) SCO coordination polymers exhibiting rich and fascinating structural features coupled to their magnetic behaviors. However, in contrast to the mononuclear compounds, these studies have been scarcely reported because of the limited number of potentially appropriate bridging anionic or neutral ligands. To the best of our knowledge, only two SCO molecular chains involving bridging anions have been reported. The first one is based on the triazolato anion and has not been fully structurally characterized;[31] the second one, reported recently, is based on an azacyanocarbanion (dicyanamide anion).[32] In this context, our strategy is to extend this polymeric approach to anionic ligands involving several potentially donating N atoms such as cyanocarbanion ligands (Scheme 1). We have reported, in the past few years, several series of magnetic coordination polymers based on various cyanocarbanions. From such studies, it was clearly established that these anions are appropriate and interesting ligands because of their high electronic delocalization and their cyano groups juxtaposed in such a way that they cannot all coordinate to the same metal ion.[33] They adopt different bridging or nonbridging coordination modes, which afford discrete as well as extended fascinating molecular architectures.

Taking into account the crucial role of these anionic ligands, we are interested in using them in combination with other chelating or bridging neutral coligands to explore the role of their structural and electronic characteristics in the field of molecular materials exhibiting the SCO phenomenon because it is governed essentially by subtle changes in the structural packing and, therefore, by the nature of the cyanocarbanion ligand. In this context, we have recently reported the first SCO series based on cyanocarbanions as the $(tcm)^-$ ($[C(CN)_3]^-$), $(tcnome)^-$, and $(tcnoet)^-$ ligands, together with abpt as the coligand (Scheme 1).[17] In this series, the single charge on the anion induces a terminal coordination mode for the cyanocarbanion unit, resulting in neutral discrete SCO complexes in which the SCO behavior is governed by the intermolecular contacts. We have clearly shown the influence of the $\pi-\pi$ stacking on their magnetic behavior. A further step in this direction would be the preparation of original extended SCO networks where the Fe^{II}abpt complexes are connected by covalent bonds. Here we show how the use of potentially bridging dianionic ligands bearing different coordination sites constitutes an original and simple method to perform this task. We report herein the synthesis, crystallographic studies of both thermally induced and photoinduced HS and LS states, and magnetic and photomagnetic properties of the first SCO iron(II) molecular neutral chain $[Fe(abpt)_2(tcpd)]$ [**1**; $(tcpd)^{2-} = [C_{10}N_6]^{2-} = (C[C(CN)_2]_3)^{2-}$ = 2-dicyanomethylene-1,1,3,3-tetracyanopropanediide anion, abpt = 4-amino-3,5-bis(pyridin-2-yl)-1,2,4-triazole] involving an anion as the bridging ligand. Note that a brief report of compound **1** has recently been communicated by us.[34]

Experimental Section

Materials. Tetracyanoethylene, urea, potassium *tert*-butoxide (C_4H_9OK), malononitrile ($CH_2(CN)_2$), 4-amino-3,5-bis(pyridin-2-yl)-1,2,4-triazole (abpt), tetramethoxysilane (TMS),

(16) Galet, A.; Gaspar, A. B.; Muñoz, M. C.; Levchenko, G.; Real, J. A. *Inorg. Chem.* **2006**, *45*, 9670–9679.
(17) Dupouy, G.; Marchivie, M.; Triki, S.; Sala-Pala, J.; Salaün, J.-Y.; Gómez-García, C. J.; Guionneau, P. *Inorg. Chem.* **2008**, *47*, 8921–8931.
(18) Sheu, C.-F.; Pillet, S.; Lin, Y.-C.; Chen, S.-M.; Hsu, I.-J.; Lecomte, C.; Wang, Y. *Inorg. Chem.* **2008**, *47*, 10866–10874.
(19) El Hajj, F.; Sebki, G.; Patinec, V.; Marchivie, M.; Triki, S.; Handel, H.; Yefsah, S.; Tripier, R.; Gómez-García, C. J.; Coronado, E. *Inorg. Chem.* **2009**, *48*, 10416–10423.
(20) Weber, B.; Bauer, W.; Obel, J. *Angew. Chem., Int. Ed.* **2008**, *47*, 10098–10101.
(21) Weber, B.; Kaps, E.; Weigand, J.; Carbonera, C.; Létard, J.-F.; Achterhold, K.; Parak, F.-G. *Inorg. Chem.* **2008**, *47*, 487–496.
(22) Reger, D. L.; Gardinier, J. R.; Elgin, J. D.; Smith, M. D.; Hautot, D.; Long, G. J.; Grandjean, F. *Inorg. Chem.* **2006**, *45*, 8862–8875.
(23) Weber, B.; Jäger, E.-G. *Eur. J. Inorg. Chem.* **2009**, 465–477.
(24) Vreugdenhil, W.; van Diemen, J. H.; de Graaff, R. A. G.; Haasnoot, J. G.; Reedjik, J.; van Der Kraan, A. M.; Kahn, O.; Zarembowitch, J. *Polyhedron* **1990**, *9*, 2971–2979.
(25) Kahn, O.; Martinez, C. J. *Science* **1998**, *279*, 44–48.
(26) Garcia, Y.; Kahn, O.; Rabardel, L.; Chansou, B.; Salmon, L.; Tuchagues, J.-P. *Inorg. Chem.* **1999**, *38*, 4663–4670.
(27) Matouzenko, G. S.; Molnár, G.; Bréfuel, N.; Perrin, M.; Bousseksou, A.; Borshch, S. A. *Chem. Mater.* **2003**, *15*, 550–556.
(28) Moliner, N.; Muñoz, M. C.; Létard, S.; Salmon, L.; Tuchagues, J.-P.; Bousseksou, A.; Real, J. A. *Inorg. Chem.* **2002**, *41*, 6997–7005.
(29) Real, J. A.; Gaspar, A. B.; Niel, V.; Muñoz, M. C. *Coord. Chem. Rev.* **2003**, *236*, 121–141.
(30) Murray, K. S.; Kepert, C. J. *Top. Curr. Chem.* **2004**, *233*, 195–228.
(31) Haasnoot, J. G.; Vos, J. G.; Groeneveld, W. L. *Z. Naturforsch. B* **1977**, *32*, 14211430.
(32) Genre, C.; Jeanneau, E.; Bousseksou, A.; Luneau, D.; Borshch, S. A.; Matouzenko, G. S. *Chem.—Eur. J.* **2008**, *14*, 697–705.
(33) Benmansour, S.; Atmani, C.; Setifi, F.; Triki, S.; Marchivie, M.; Gómez-García, C. J. *Coord. Chem. Rev.* **2010**, *254*, 1468–1478.
(34) Dupouy, G.; Marchivie, M.; Triki, S.; Sala-Pala, J.; Gómez-García, C. J.; Pillet, S.; Lecomte, C.; Létard, J.-F. *Chem. Commun.* **2009**, 3404–3406.

$FeCl_2 \cdot 4H_2O$, and $Fe(BF_4)_2 \cdot 6H_2O$ were purchased from commercial sources and used without further purification. Solvents were used and purified by standard procedures. The potassium salt K_2(tcpd) was prepared according to ref 35; the corresponding tetrabutylammonium salt was prepared by metathesis in aqueous solution.

Synthesis. To an aqueous solution (10 mL) of $K_2(tcpd) \cdot 2H_2O$ (84.0 mg, 0.25 mmol) was added, under vigorous stirring, 1.0 mL of TMS. A gel formed upon standing 1 day at room temperature. A methanolic solution (10.0 mL) containing $FeCl_2 \cdot 4H_2O$ (0.050 g, 0.25 mmol) and abpt (15.0 mg, 0.063 mmol) was carefully added onto the gel. Yellow prismatic single crystals of **1** and a microcrystalline red product (**2**) were obtained simultaneously within the gel at room temperature after several weeks. Because compound **2** appears as a microcrystalline powder, yellow crystals of compound **1** were easily separated as the major product. The single crystals were then washed with cold water and dried in air (yield 22%). In order to settle specific experimental procedures to selectively obtain each compound, we performed the synthesis using slow diffusion in an H tube containing an aqueous solution of $Fe(BF_4)_2 \cdot 6H_2O$ (33.75 mg, 0.10 mmol) and $K_2(tcpd) \cdot 2H_2O$ (31.84 mg, 0.10 mmol) in one arm and a methanolic solution of abpt (23,8 mg, 0.10 mmol) in the other one. Dark-red prismatic crystals of compound **2** were obtained as the unique product upon standing 6 weeks at room temperature. The crystals were washed with cold water and dried in air (yield 59%). Elem anal. Calcd for **1** ($C_{34}H_{20}N_{18}Fe$): C, 55.5; H, 2.7; N, 34.2; Fe, 7.6. Found: C, 55.7; H, 2.6; N, 34.1; Fe, 7.4. Calcd for **2** ($C_{47}H_{36}N_{24}O_2Fe$): C, 55.1; H, 3.5; N, 32.8; Fe, 5.5. Found: C, 55.4; H, 3.4; N, 32.3; Fe, 5.8. IR absorptions (KBr; ν/cm^{-1}): 3426br, 3281w, 3199w, 2925w, 2187s, 2175m, 2168m, 2122m, 1653w, 1635w, 1602w, 1591w, 1570w, 1490w, 1458w, 1451w, 1431s, 1413s, 1296w, 1254w, 1035w, 792w, 748w, 701w for **1**; 3384br, 3253m, 3139m, 2181s, 2159s, 2110m, 1653, 1608w, 1590m, 1572w, 1454s, 1423s, 1403s, 1286w, 1249w, 1151w, 1028m, 1003m, 792s, 756m, 695m, 613m, 539w for single crystals of **2**.

Physical Measurements. IR spectra were recorded in the range 4000−200 cm^{-1} as KBr pellets on a Nicolet Nexus FT-IR spectrometer. Variable-temperature susceptibility measurements for compound **1** were carried out in the temperature range 2−300 K with an applied magnetic field of 0.1 T on a polycrystalline sample (mass = 35.53 mg) with a Quantum Design MPMS-XL-5 SQUID magnetometer. The susceptibility data were corrected for the sample holders previously measured using the same conditions and for the diamagnetic contributions of the salt as deduced by using Pascal's constant tables ($\chi_{dia} = -464.6 \times 10^{-6}$ emu·mol^{-1}). Elemental analyses were obtained from the Service Central d'Analyses (Vernaison, France). The photomagnetic characterization of compound **1** was carried out using a Kr^+ laser coupled through an optical fiber into the cavity of a Quantum Design MPMS-55 SQUID magnetometer operating at 2 T. The sample was prepared as a thin layer (≈0.1 mg) to promote full penetration of the irradiating light. The sample weight was obtained by comparing its thermal spin transition behavior with a heavier and accurately weighed sample.[6] The sample was first slowly cooled to 10 K, ensuring that potential trapping of HS species at low temperatures did not occur. Irradiation was carried out several times using different wavelengths (i.e., 337/356.4, 406.7/415.4, 514, 647.1/676.4, and 752.5/799.3 nm) and power intensities of up to 5 mW·cm^{-2} to determine the most efficient conditions to reach a high LS-to-HS conversion yield at photosaturation. The sample in the LS state was then irradiated with green light (λ = 514 nm, 5 mW·cm^{-2}), which proved to be the most efficient, until photosaturation was reached. After irradiation was switched off, the temperature was increased at a rate of 0.3 K·min^{-1} to 100 K, to determine the T(LIESST) value,[6,49,50] and over the range 100−300−10 K, to follow the thermal spin transition. The T(*LIESST*) value was determined as the minimum of the $\partial\chi_m T/\partial T$ vs T plot (the maximum slope in the $\chi_m T$ vs T plot), corresponding to the temperature at which the light-induced HS information is erased.[6] For the kinetic study, the sample was irradiated at 10 K until photosaturation, and then the temperature was set to 10, 20, 25, 30, 35, and 40 K and the light was switched off in order to study the relaxation kinetics. Reverse-LIESST experiments were performed by irradiating the sample at 10 K with a 830 nm diode laser (5 mW·cm^{-2}).

X-ray Crystallography. Selected single crystals were embodied in vacuum grease and mounted on a glass fiber. The diffraction data of **1** were collected at 293, 200, 150, 100, and 10 K after thermal quenching, at 10 K in the light-induced metastable HS state, and at 10 K after subsequent relaxation from the thermally quenched metastable HS state, using an Oxford Diffraction Xcalibur CCD diffractometer with Mo Kα radiation, equipped with the required cooling system (nitrogen open-flow cryostream for the temperature range 293−100 K and helium open-flow Oxford diffraction Helijet for the temperature range 45−10 K). A helium open-flow cryosystem used for all of the 10 K experiments restricts the available angular range of the goniometer and the detector-to-crystal distance, which correlatively prevents one from reaching 100% completeness in a low-symmetry crystal system. However, 70% completeness could be reached in all 10 K measurements, leading to relatively good quality crystal structures (Table 1). Photoexcitation was performed using an argon−krypton gas laser tuned to λ = 534 nm with continuous rotation of the crystal to enhance the photoexcitation efficiency. The unit cell determination and data reduction were performed using the *CrysAlis* program suite[36] on the full set of data. The crystal structures were solved by direct methods and successive Fourier difference syntheses with the *Sir97* program[37] and refined on F^2 by weighted full-matrix least-squares methods using the *SHELXL97* program.[38] Both programs were used within the *WINGX* package.[39] Compound **1** crystallizes in the monoclinic space group $P2_1/n$ and does not show any structural phase transition within the measured temperature range. The $(tcpd)^{2-}$ anion presents an orientation disorder persisting even at 10 K. Both orientations appear in the asymmetric unit as halves of the $(tcpd)^{2-}$ anion in a 0.5/0.5 occupation ratio. The C16 atom is common to both orientations and has, therefore, an occupancy factor of 1. To better understand the structural changes occurring during the LIESST effect, we have also measured the thermal variation of the unit cell volume of **1** under continuous irradiation (λ = 534 nm). The cell parameters were first measured by increasing the temperature from 10 to 45 K under continuous irradiation and then cooling from 45 to 10 K without irradiation (Figures 1 and 10).

The unit cell parameters, crystal data, and refinement details are summarized in Table 1. The relevant structural modifications induced by temperature variation and light irradiation are given in Table 2.

Results and Discussion

Synthesis and General Characterization of 1. Diffusion, at room temperature, of a methanolic solution

(35) Middleton, W. J.; Little, E. L.; Coffman, D. D.; Engelhardt, V. A. *J. Am. Chem. Soc.* **1958**, *80*, 2795–2809.

(36) *Xcalibur CCD system, CrysAlis Software system*, version 1.171; Oxford Diffraction Ltd.: Oxford, U.K., 2005.

(37) Altomare, A.; Burla, M. C.; Camalli, M.; Cascarano, C.; Giacovazzo, C.; Guagliardi, A.; Moliterni, A. G. G.; Polidori, G.; Spagna, R. *J. Appl. Crystallogr.* **1999**, *32*, 115–119.

(38) Sheldrick, G. M. *SHELX97, Programs for Crystal Structure Analysis*; University of Göttingen: Göttingen, Germany, 1997.

(39) Farrugia, L. J. *J. Appl. Crystallogr.* **1999**, *32*, 837–838.

Table 1. X-ray Data Collection and Refinement Details for **1** in the Temperature Range 293−10 K

	293 K	200 K	150 K	100 K	10 K "flash cooled"	10 K "light induced"	10 K "relaxed state"
color	yellow	yellow	yellow	red	red	yellow	red
formula[a]				$C_{34}H_{20}N_{18}Fe$			
fw ($g \cdot mol^{-1}$)				736.53			
cryst syst				monoclinic			
space group				$P2_1/n$ (No. 14)			
a (Å)	11.3762(3)	11.3665(1)	11.3439(2)	11.2359(3)	11.2071(8)	11.3894(8)	11.1139(2)
b (Å)	12.4222(3)	12.2759(2)	12.2258(2)	12.2079(2)	12.1518(6)	12.1165(4)	12.1722(3)
c (Å)	11.8683(3)	11.8437(1)	11.8418(2)	11.8655(2)	11.8916(5)	11.8384(4)	11.8855(2)
β (deg)	92.031(2)	92.364(1)	92.401(1)	91.703(2)	91.495(5)	92.832(4)	90.866(2)
V (Å^3)	1676.14(7)	1651.19(3)	1640.89(3)	1626.83(6)	1618.9(2)	1631.70(14)	1607.69(6)
Z[a]	2	2	2	2	2	2	2
ρ_{calcd}	1.459	1.481	1.491	1.504	1.511	1.499	1.521
μ (mm^{-1})	0.507	0.514	0.518	0.522	0.525	0.520	0.528
F_{000}	752	752	752	752	752	752	752
cryst size (mm)	0.33 × 0.09 × 0.09	0.32 × 0.20 × 0.16		0.33 × 0.09 × 0.09	0.24 × 0.12 × 0.12		0.39 × 0.19 × 0.17
reflns measured	18122	28702	13426	21459	7010	6258	8194
2θ range	5.88−46.50	6.64−66.28	6.64−66.28	5.94−52.74	5.96−52.96	5.90−52.72	6.0−65.02
reflns unique/R_{int}	2390/0.0275	6276/0.026	6239/0.018	3234/0.0311	2474/0.0457	2337/0.0267	4596/0.0257
reflns with $I > 2\sigma(I)$	1858	5610	5592	2353	1514	1747	3813
$N_{var.}$	332	322	322	322	297	288	312
R1[b]/wR2[c]	0.0353/0.0747	0.067/0.133	0.074/0.148	0.0417/0.0839	0.0485/0.0810	0.0483/0.0892	0.0789/0.1608
GOF[d]	1.112	1.282	1.364	1.110	1.040	1.144	1.286
$\Delta\rho_{max,min}$/e·Å^{-3}	0.202/−0.137	0.361/−0.536	0.422/−0.676	0.285/−0.250	0.333/−0.296	0.423/−0.288	0.779/−0.964

[a] The asymmetric unit contains 0.5 of the chemical formula. [b] $R1 = \sum|F_o - F_c|/F_o$. [c] $wR2 = \{\sum[w(F_o^2 - F_c^2)^2]/\sum w(F_o^2)^2]\}^{1/2}$. [d] $GOF = \{\sum[w(F_o^2 - F_c^2)^2]/(N_{obs} - N_{var.})\}^{1/2}$.

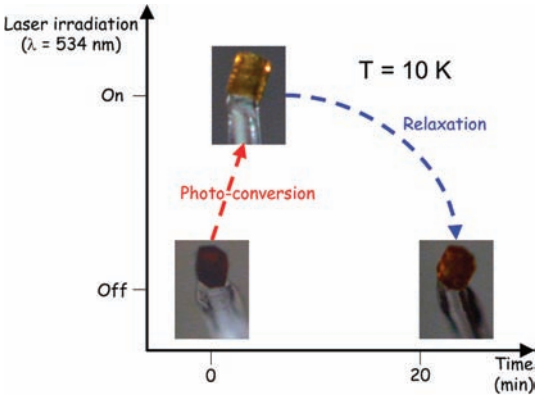

Figure 1. Snapshots of the single crystal during the photocrystallographic experiment showing the photochromic effect (dark red and yellow correspond to the LS and HS states, respectively).

containing $FeCl_2 \cdot 4H_2O$ and abpt through a silicate gel of $K_2(tcpd) \cdot 2H_2O$ in 1:2:1 ratio respectively affords, after several weeks, a mixture of yellow single crystals (**1**) and a red microcrystalline powder (**2**). In order to obtain compound **1** as the unique product, we performed several syntheses with different Fe^{II}/abpt ratios. Unfortunately, in all cases, a mixture of both compounds was obtained. However, as described in the Experimental Section, using a $Fe^{II}/(tcpd)^{2-}$/abpt ratio of 4:4:1 afforded compound **1** as the major product. This result indicates, on one hand, that a high Fe^{II}/abpt ratio (1:1) favors the formation of **1** and suggests, on the other hand, that the formation of the red product (**2**) requires a lower Fe^{II}/abpt ratio. In order to improve the yield of compound **1** and to obtain it selectively, we have performed alternative syntheses by slow diffusion in an H tube with different Fe^{II}/abpt ratios. As mentioned in the Experimental Section, this procedure only affords compound **2**. Thus, the diffusion method through the silicate gel appears to be the only experimental method that allows formation of **1**. Although diffusion in H tubes failed to obtain compound **1**, it has allowed the synthesis of single crystals of **2** as the unique product. The crystal structure determination of **2** showed that this compound corresponds to $[Fe(abpt)_3](tcpd)(CH_3OH)(H_2O)$[40] in which the cyanocarbanion is not coordinated to the metal. The $[Fe(abpt)_3]^{3+}$ complex presents a lower Fe^{II}/abpt ratio (1:3) than compound **1** (1:2), in agreement with the synthetic procedure described above. Compounds **1** and **2** display similar IR patterns. As expected, both show several absorption bands assigned to the ν_{CN} stretching vibrations (2122m, 2168m, 2175m, and 2187s cm^{-1} for **1** and 2110m, 2159s, and 2181s cm^{-1} for **2**). The slight shift to higher wavenumbers of ca. 10 cm^{-1} observed for the absorption bands of **1** may be attributed to coordination of some CN groups in **1** in contrast to the uncoordinated cyanocarbanion in **2**, as confirmed by X-ray structural analyses (see below).

Crystal Structure Description. The following general structural description is relative to the room temperature data; the relevant structural modifications induced by variation of the temperature and/or by light irradiation will be discussed further in the following sections. The structure of **1** is built from one Fe^{II} ion, one $(tcpd)^{2-}$ anion, both located on inversion centers, and one chelating abpt ligand located on a general position. The $(tcpd)^{2-}$

(40) Crystal data for **2**: $C_{47}H_{36}N_{24}O_2Fe$, M = 1024.85, triclinic, space group $P\bar{1}$, Z = 2, T = 170 K, red color, a = 8.3083(6) Å, b = 14.3558(11) Å, c = 20.1709(14) Å, α = 81.591(6)°, β = 84.044(6)°, γ = 80.621(6)°, V = 2340.3(3) Å^3, D_{calcd} = 1.454 g·cm^{-3}, 20 259 collected reflections, 12 949 unique (R_{int} = 0.0906), R1 = 0.0699, wR2 = 0.1135, R indices based on 4016 reflections with $I > 2\sigma(I)$, 666 parameters. The asymmetric unit of **2** is formed by one $[Fe(abpt)_3]^{2+}$ cation, one $(tcpd)^{2-}$ anion, one water molecule, and one CH_3OH molecule, all located on the general position. The average value of the six Fe−N distances [1.958(3) Å] is in good agreement with the values expected for LS iron(II) complexes in distorted octahedral geometry. CCDC 751546 contains the supplementary crystallographic data for this complex.

Table 2. Selected Bond Lengths (Å), Bond Angles (deg), and Distortion Parameters (deg) of the Iron(II) Coordination Sphere for **1** in Different Spin States and Temperature Conditions

			T = 10 K		
	T = 293 K	T = 100 K	flash cooled	light induced	relaxed state
Fe1−N1	2.187(2)	2.114(2)	2.091(3)	2.179(3)	2.061(3)
Fe1−N2	2.113(2)	2.060(2)	2.047(3)	2.113(3)	2.008(3)
Fe1−N3	2.176(2)	2.075(2)	2.056(3)	2.175(3)	1.985(3)
⟨Fe−N⟩	2.159(2)	2.083(2)	2.065(3)	2.156(3)	2.018(3)
N1−Fe−N2	76.53(8)	78.18(8)	78.65(12)	77.00(10)	79.56(12)
N1−Fe−N2^a	103.47(8)	101.82(8)	101.35(12)	103.00(10)	100.44(12)
N1−Fe−N3	90.95(8)	91.77(8)	92.04(12)	91.02(11)	92.34(12)
N1−Fe−N3^a	89.05(8)	88.23(8)	87.96(12)	88.98(11)	87.66(12)
N2−Fe−N3	86.00(8)	86.05(7)	86.08(10)	85.59(11)	85.98(11)
N2−Fe−N3^a	94.00(8)	93.95(7)	93.92(10)	94.41(11)	94.02(11)
Σ^a	74(1)	70(1)	69(2)	74(2)	67(2)
Θ^b	246(2)	220(2)	212(3)	241(3)	196(3)

^{a} Σ[47] is the sum of the deviation from 90° of the 12 cis angles of the FeN_6 octahedron. ^{b} Θ[48] is the sum of the deviation from 60° of the 24 trigonal angles of the projection of the FeN_6 octahedron onto its trigonal faces.

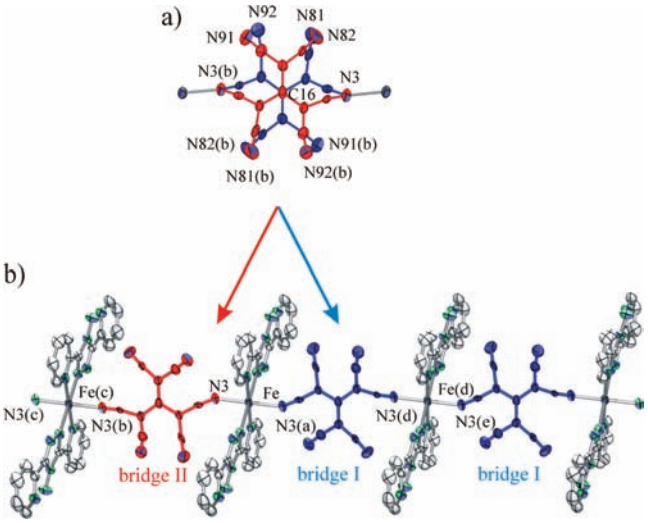

Figure 2. (a) ORTEP plot of the disordered bridging $(tcpd)^{2-}$ anion showing the two orientations (bridge I in blue and bridge II in red). (b) ORTEP perspective view of one hypothetic fragment of the 1D structure of **1** at 293 K showing the two possible local environments for iron. Code of equivalent positions: (a) $1-x, 2-y, -z$; (b) $2-x, 2-y, -z$; (c) $1+x, y, z$; (d) $-1+x, y, z$; (e) $-x, 2-y, -z$.

anion is, furthermore, completely disordered over two orientations, with the central atom C16 being located on the inversion center (Figure 2a). C16 is common to both orientations. As shown in Figure 2b, the Fe^{II} ion adopts an FeN_4N_2 distorted octahedral geometry with four equatorial N atoms from two abpt chelating ligands (N1, N2, N1a, and N2a) and two axial N atoms (N3 and N3a) from the $(tcpd)^{2-}$ ligand. Selected bond lengths and angles for the iron coordination sphere are summarized in Table 2.

At room temperature, the average value of the six Fe−N distances [2.159(2) Å] is in good agreement with the value expected for HS iron(II) complexes in distorted octahedral geometry.[17,40] The bond lengths and angles of the $(tcpd)^{2-}$ anion are in the same range as those observed in other coordination complexes involving this anion.[41,42] The trigonal distortion of the octahedral iron(II) environment is highlighted by the Σ and Θ parameters, which are defined as the sum of the deviation from 90° of the 12 cis N−Fe−N angles and the deviation from 60° of the 24 trigonal angles on the projection of the octahedron onto its trigonal faces, respectively. Relatively high values of the Σ and Θ parameters are observed here at room temperature, indicative of a high degree of distortion of the FeN_6 octahedron, typical for a HS coordination sphere.

The crystal packing of **1** is built from regular chains running along the crystallographic a axis, in which the cyanocarbanion $(tcpd)^{2-}$ acts as a μ_2-bridging ligand via two N atoms of two different $-C(CN)_2$ wings (Figure 2b). The orientation disorder of the bridging ligand leads formally to two distinct local coordination geometries of the central Fe^{II} cation: one in which the $(tcpd)^{2-}$ ligands adopt the same orientation (see Fe(d) in Figure 2b) and one in which they adopt both orientations (see Fe in Figure 2b). As a consequence, the overall crystal structure may be pictured as formed by chains presenting statistically distributed mixtures of both orientations of the anionic ligand and thus a statistical distribution of both types of iron(II) coordination geometries. This assumption is clearly supported by the crystallographic data because all attempts to solve the crystal structure in the corresponding noncentrosymmetric space group (Pn, $P2_1$, and $P1$), that is to say, releasing the inversion center located on C16, led us systematically to the statistical disorder showing the same two orientations of the $(tcpd)^{2-}$ ligand. Along the chains, the Fe···Fe separation distance is simply given by the length of the crystallographic a axis, while the closest interchain contacts are directed along the [011] and [01−1] directions.

The amino group of the abpt ligand is involved in a number of intrachain hydrogen bonds: two weak, namely, N6−H1N···N7 [2.834(4) Å] and C4−H4···N6 [3.048(5) Å] within the abpt ligand, and two moderate, N6−H2N···N81 [3.28(3) Å] and N6−H2N···N82 [3.15(3) Å], with the two orientations of the $(tcpd)^{2-}$ anion. The latter are most probably at the origin of the disorder of the $(tcpd)^{2-}$ group in the following way. N6−H2N···N82 [3.15(3) Å] is slightly shorter than N6−H2N···N81 [3.28(3) Å], so that one single orientation cannot lead at the same time to two moderate hydrogen bonds. On the contrary, each orientation of

(41) Triki, S.; Thétiot, F.; Vandevelde, F.; Sala-Pala, J.; Gómez-Garcia, C. J. *Inorg. Chem.* **2005**, *44*, 4086–4093.
(42) Triki, S.; Sala-Pala, J.; Decoster, M.; Molinié, P.; Toupet, L. *Angew. Chem., Int. Ed.* **1999**, *38*, 113–115.

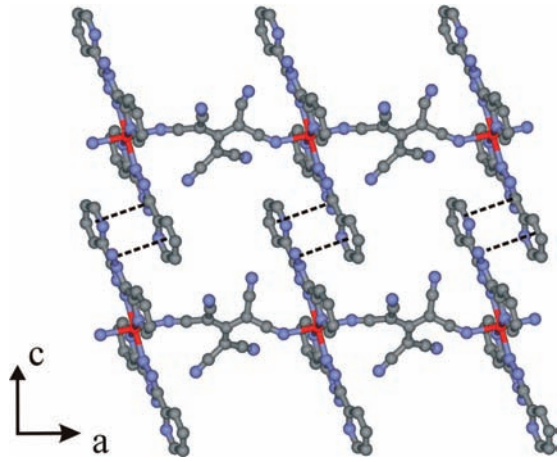

Figure 3. Packing diagram of **1** in the *ac* plane showing the predominant $\pi-\pi$ interactions between the abpt ligands of adjacent chains along the *c* crystallographic axis. Only one contribution to the orientation disorder of the $(tcpd)^{2-}$ ligands is depicted for clarity.

the $(tcpd)^{2-}$ ligand leads to one moderate and one weak hydrogen bond. Careful examination of the crystal packing in **1** reveals that the main interchain contacts are due to π-stacking interactions between two abpt ligands. As clearly depicted in Figure 3, such $\pi-\pi$ interactions between the abpt ligands of adjacent chains are similar to those observed in the parent discrete complexes of the $[Fe(abpt)_2(A)_2]$ series (A = monoanionic cyanocarbanion) reported recently.[17] The efficiency of these interactions (at least five short C−C or C−N contacts in the range 3.26−3.55 Å) is similar to that observed in the SCO complexes of the $[Fe(abpt)_2(A)_2]$ series and induces a more planar abpt ligand (dihedral angle $\sim$ 14.9°) as compared with those observed in non-SCO complexes of this family, which systematically adopt a sideways overlap mode with a less efficient abpt stacking.[17] This observation is in agreement with the magnetic behavior of **1** (see below) and confirms the crucial role played by the abpt−abpt π interactions in the presence of the SCO transition in these Fe^{II}abpt complexes. In addition to these predominant π-stacking interactions, the interchain contacts also involve hydrogen bonds between the amino group of the abpt ligand and the N91 atoms of the tcpd groups of adjacent chains [N6−H1N···N91 = 3.036(9) Å], as well as weak C2−H2···N81 hydrogen bonds [C2−H2···N81 = 3.25(3) Å].

Thermomagnetic Properties. The room temperature value of the product of the molar magnetic susceptibility times the temperature per Fe^{II} ion ($\chi_m T$ = 3.45 $cm^3 \cdot K \cdot mol^{-1}$) is the expected one for an isolated S = 2 Fe^{II} ion with a g value of ca. 2.14. When the sample is cooled, the $\chi_m T$ product remains constant down to ca. 170 K, and below this temperature, it shows a progressive decrease with a tiny change of slope at ca. 100 K to reach a plateau of ca. 1.0 $cm^3 \cdot K \cdot mol^{-1}$ at ca. 50 K (Figure 4).

This progressive decrease observed between 170 and 50 K indicates the presence of an incomplete HS/LS SCO transition. The remaining $\chi_m T$ value of ca. 1 $cm^3 \cdot K \cdot mol^{-1}$ indicates that at low temperatures there exists a fraction of ca. 25% of residual Fe^{II} ions in the HS configuration. In the temperature range 50−10 K, the $\chi_m T$ product remains constant, indicative of a paramagnetic behavior of the residual HS iron(II) species. Below ca. 10 K, it shows an abrupt decrease, reaching a value of ca. 0.8 $cm^3 \cdot K \cdot mol^{-1}$ at 2 K, which can be attributed to the presence of a zero-field splitting of the residual HS iron(II) species and/or to the presence of a weak antiferromagnetic coupling between the residual HS iron(II) species through the $(tcpd)^{2-}$ bridge. As was already mentioned, a careful inspection of the decrease of the $\chi_m T$ product in the temperature range 170−50 K shows a tiny change of slope with two inflection points at ca. 100 and 60 K. These changes are readily detected in the thermal variation of the derivative of the $\chi_m T$ product with respect to the temperature (inset in Figure 4), which shows two different maxima at ca. 105 and 60 K. The presence of these maxima indicates that there are two different transition temperatures ($T_{1/2}$) for the SCO transition.

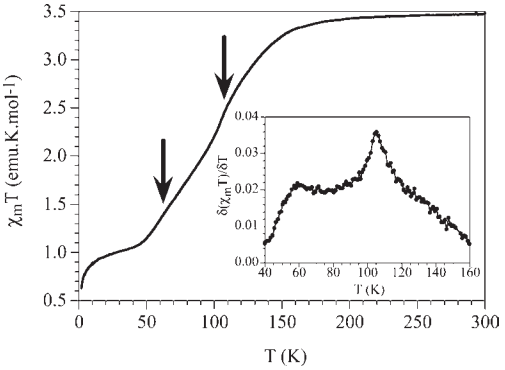

Figure 4. Thermal variation of the $\chi_m T$ product of **1** showing the gradual two-step spin transition. The arrows indicate the two inflection points in the SCO transition. Inset: derivative of the $\chi_m T$ product as a function of the temperature, indicating the presence of two maxima at ca. 60 and 105 K.

Photomagnetic Properties. The complete photomagnetic study performed on **1** shows that irradiation at 10 K with a green laser light (λ = 514 nm, 5 $mW \cdot cm^{-2}$) resulted in a large increase of the magnetic signal (Figure 5). After 1 h of irradiation, the light was switched off and the temperature increased at a rate of 0.3 $K \cdot min^{-1}$, corresponding to the standard measurement of the T(LIESST) temperature.[6,59,50] On the basis of this experiment, several remarks follow. The small decrease of the magnetic signal recorded below 25 K can be attributed either to the zero-field splitting of the individual photoinduced HS state or to a small antiferromagnetic coupling between the Fe^{II} ions in the HS state in the chain, as reported, with a larger magnitude, for other iron(II)

(43) Real, J. A.; Bolvin, H.; Bousseksou, A.; Dworkin, A.; Kahn, O.; Varret, F.; Zarembowitch, J. *J. Am. Chem. Soc.* **1992**, *114*, 4650–4658.
(44) Bousseksou, A.; Molnár, G.; Real, J. A.; Tanaka, K. *Coord. Chem. Rev.* **2007**, *251*, 1822–1833.
(45) Neville, S. M.; Leita, B. A.; Halder, G. J.; Kepert, C. J.; Moubaraki, B.; Létard, J.-F.; Murray, K. S. *Chem.—Eur. J.* **2008**, *14*, 10123–10133.
(46) Guionneau, P.; Marchivie, M.; Bravic, G.; Létard, J.-F.; Chasseau, D. *Top. Curr. Chem.* **2004**, *234*, 97–128.
(47) Guionneau, P.; Brigouleix, C.; Barrans, Y.; Goeta, A. E.; Létard, J.-F.; Howard, J. A. K.; Gaultier, J.; Chasseau, D. *C.R. Acad. Sci., Ser. IIc: Chim.* **2001**, *4*, 161–171.
(48) Marchivie, M.; Guionneau, P.; Létard, J.-F.; Chasseau, D. *Acta Crystallogr., Sect. B* **2003**, *59*, 479–486.
(49) Létard, J.-F.; Guionneau, P.; Rabardel, L.; Howard, J. A. K.; Goeta, A. E.; Chasseau, D.; Kahn, O. *Inorg. Chem.* **1998**, *37*, 4432–4441.
(50) Létard, J.-F.; Guionneau, P.; Nguyen, O.; Costa, J. S.; Marcén, S.; Chastanet, G.; Marchivie, M.; Capes, L. *Chem.—Eur. J.* **2005**, *11*, 4582–4589.

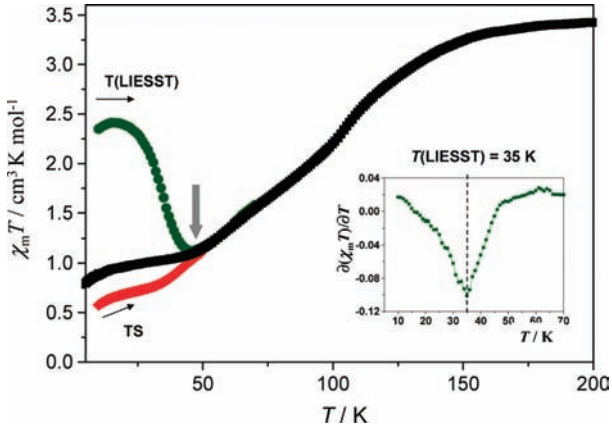

Figure 5. Plot of $\chi_m T$ versus temperature over the range 10−200 K showing the thermo- and photomagnetic properties of compound **1**. Inset: Plot of $\partial\chi_m T/\partial T$ versus temperature indicating the T(LIESST) value of 35 K at the minimum. The gray arrow symbolizes the crossing point between the thermal spin transition, the metastable LIESST, and the reverse-LIESST regimes.

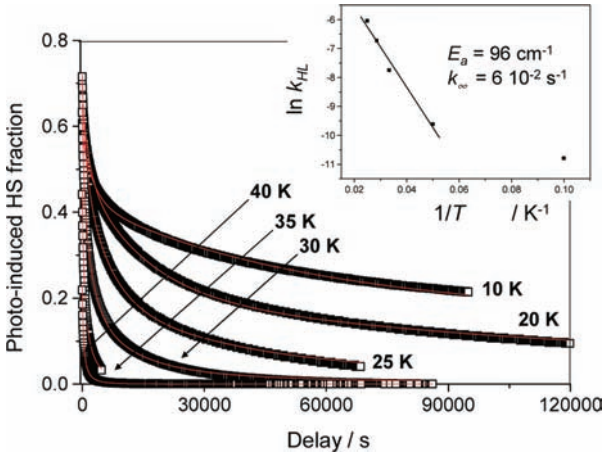

Figure 6. Plot of the HS fraction versus time for compound **1** of the relaxation kinetics at 10, 20, 25, 30, 35, and 40 K of the light-induced metastable HS state. Inset: pseudo-Arrhenius plot ln k_{HL} versus $1/T$.

dinuclear complexes[51−53] and for some chain compounds with the same bridging $(tcpd)^{2-}$ ligand.[17,54] However, according to these last compounds, antiferromagnetic coupling, if present, should be weak.

The comparison between the maximum of the T(LIESST) curve and the value of the magnetic moment at high temperature, where the system is in a 100% HS state, indicates that at low temperatures the photoconversion reaches ca. 70% of the HS state in the bulk material. Note that increasing the irradiation time and intensity and/or changing the wavelength of excitation did not enhance the photoexcitation yield. Because the color of the sample is basically not so deep, the problem of the light penetration depth can be ruled out. This effect may rather be attributed to a competition between photoexcitation and an efficient photoinduced HS/LS relaxation process, as illustrated by the relatively small T(LIESST) of 35 K and by the efficiency of the photoinduced HS/LS relaxation process recorded at 10 K. This last relaxation process concerns the light-trapped HS state, which relaxes back to the original thermal spin transition curve rather than to a fully LS state (as is also shown by the crystal structure of the relaxed state at 10 K, see below). This confirms that the incompleteness of the SCO in this compound is not caused by kinetic trapping of a high-spin fraction of the sample at low temperatures, as was recently reported for the $[FeL_2][BF_4]_2 \cdot xH_2O$ complex [L = 2,6-bis(3-methylpyrazol-1-yl)pyridine; $x = 0-{}^1/_3$].[55]

Figure 6 displays the decay kinetics for the metastable LIESST state recorded in the 10−40 K temperature range. As expected, the relaxation rates increase with temperature. The most striking feature of these relaxation curves is the strong deviation from single exponential, with a marked stretched exponential behavior with a fast component at earlier times and a long decay process at infinite times. Such stretched exponential behaviors have already been mentioned in disordered systems, like an iron(II) SCO complex dispersed into a polymer matrix[56] or organized on a surface by the Langmuir−Blodgett technique.[57] For reproducing these types of curves, Hauser[58] introduced a distribution of relaxation rates at a given temperature with a Gaussian distribution of the activation energy. Following this procedure, the relaxation curves of compound **1** can be satisfactorily fitted, as illustrated by the solid lines in Figure 6, with the parameters shown in Table 3.

Table 3. Kinetic Parameters of the Photoinduced HS → LS Relaxation Process, with k_{HL} the Rate Constant at a Given Temperature (T) and σ the Standard Deviation in the Activation Energy According to a Gaussian Distribution

T/K	k_{HL}/s^{-1}	σ/cm^{-1}
10	2.05×10^{-5}	21
20	6.65×10^{-5}	30
30	4.29×10^{-4}	31
35	1.12×10^{-3}	27
40	2.37×10^{-3}	30

The apparent activation energy, $E_a = 96$ cm^{-1}, and the apparent pre-exponential factor, $k_\infty = 6 \times 10^{-2}$ s^{-1}, of the activated region are calculated from the straight line of the ln $k_{HL}(T)$ vs $1/T$ plot (Figure 6). The distribution width of the activation energy in a Gaussian approach is 25 ± 5 cm^{-1}.

If we now consider the HS residual fraction (of about 25%) recorded at 10 K, we can see, on the one side, that photoexcitation with a green laser induces conversion toward the metastable HS state and, on the other side, that this HS residual fraction remaining at 10 K is kinetically independent, as illustrated by the constant magnetic signal recorded in the dark over more than 2 h (Figure 7). Interestingly, by irradiating the sample with a

(51) Létard, J.-F.; Real, J. A.; Moliner, N.; Gaspar, A. B.; Capes, L.; Cador, O.; Kahn, O. *J. Am. Chem. Soc.* **1999**, *121*, 10630–10631.
(52) Chastanet, G.; Gaspar, A. B.; Real, J. A.; Létard, J.-F. *J. Chem. Soc., Chem. Commun.* **2001**, 819–820.
(53) Chastanet, G.; Carbonera, C.; Mingotaud, C.; Létard, J.-F. *J. Mater. Chem.* **2004**, *14*, 3516–3523.
(54) Thétiot, F.; Triki, S.; Sala-Pala, J.; Gómez-García, C. J. *Synth. Met.* **2005**, *153*, 481–484.
(55) Money, V. A.; Carbonera, C.; Halcrow, M. A.; Howard, J. A. K.; Létard, J.-F. *Chem.—Eur. J.* **2007**, *13*, 5503–5514.
(56) Hauser, A.; Adler, J.; Gütlich, P. *Chem. Phys. Lett.* **1988**, *152*, 468–472.
(57) Létard, J.-F.; Nguyen, O.; Soyer, H.; Mingotaud, C.; Delhaès, P.; Kahn, O. *Inorg. Chem.* **1999**, *38*, 3020–3021.
(58) Hauser, A. *Chem. Phys. Lett.* **1986**, *124*, 543–548.

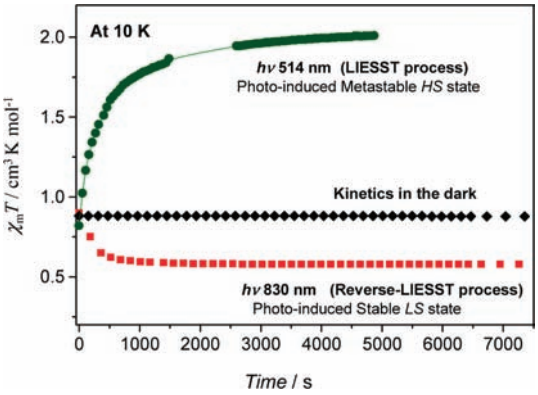

Figure 7. Time dependence of the magnetic signal at 10 K in the dark and under light irradiation at 514 and 830 nm.

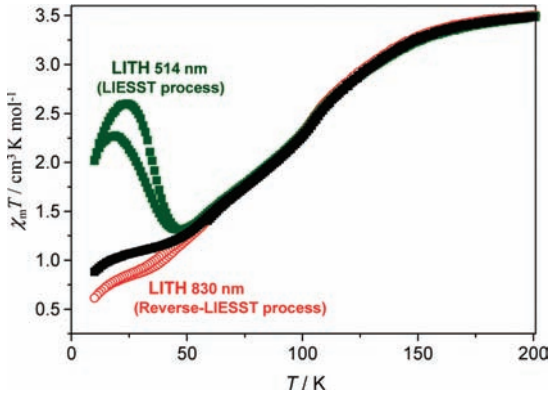

Figure 8. LITH experiments performed under constant irradiation at 514 and 830 nm.

laser diode emitting at 830 nm, we observe a decrease of the magnetic signal, suggesting that the reverse-LIESST effect[58] can be induced in this class of compounds. On that basis, Figure 8 shows the two light-induced thermal hysteresis[49] (LITH) curves recorded by cooling and warming of the sample under constant irradiation at 514 and 830 nm. In the former case, the curve displays a minor apparent hysteresis, while in the latter case, the use of a constant 830 nm irradiation allows one to partially complete the thermal spin conversion down to nearly 15% of the HS residual faction.

Thermo- and Photocrystallographic Analysis. On the basis of the conclusions drawn from the magnetic and photomagnetic data, the crystal structure of **1** has been determined at various temperatures and different laser illumination conditions: at 298, 200, and 150 K in the cooling mode, at 100 K close to the inflection point of the thermomagnetic curve (hereafter called the intermediate phase), at 10 K after thermal quenching, at 10 K after thermal relaxation, and at 10 K after laser light excitation. The corresponding structural parameters are collected in Table 2. Some of these parameters, such as the average coordination distance ⟨Fe−N⟩ and the trigonal distortion parameters Σ and Θ (see above for their definitions), are known to be highly sensitive on the iron(II) spin configuration and will thus be used hereafter to assign the spin state on each crystallographic Fe site ($\langle Fe-N\rangle_{LS} \sim 2.0$ Å; $\langle Fe-N\rangle_{HS} \sim 2.2$ Å). It is important to mention that the crystal structure of **1** at room temperature presents only one crystallographically independent Fe^{II} site and that, for all of the other crystal structures that we derived in the present study, no symmetry change (cell doubling or space group change) occurs. This means that, in the characterized mixed spin states ($0.0 < \gamma_{HS} < 1.0$) for which both HS and LS species coexist, these species are statistically distributed along the one-dimensional (1D) structural chains. This assertion is supported by the absence of any specific HS/LS crystallographic long-range ordering, which would have been evidenced by superstructure reflections or diffuse scattering on the diffraction pattern of the intermediate phase at 100 K (see below).

Strong modifications of the iron coordination sphere are observed while the temperature is varied in the range 293−10 K. Upon cooling from room temperature to 100 K (close to the inflection point on the thermomagnetic curve), the ⟨Fe−N⟩ parameter decreases from 2.159(2) to 2.083(2) Å. In parallel, the trigonal distortion parameters are significantly reduced, owing to the more regular FeN_6 octahedral geometry in the LS state. This trend is in agreement with the presence of a SCO transition from HS to LS in **1**. Further slow cooling to 10 K was not possible directly using our nitrogen cryosystem. Therefore, the single-crystal sample was thermally quenched from room temperature to 10 K using a Helijet open-flow helium cryosystem. Upon thermal quenching, the average coordination ⟨Fe−N⟩ distance decreases to 2.065(3) Å, which is significantly lower than the value derived at 100 K; the trigonal distortion parameters are also reduced as well. These values indicate that the corresponding HS fraction is about 50% by comparison to those expected for pure LS or pure HS states.[46] Such an observation suggests the presence of a thermally trapped metastable HS state at low temperatures because magnetic data indicate a lower residual HS fraction of only ca. 25% at 10 K. The sample was then heated up to 60 K in order to induce the HS to LS relaxation and further cooled to 10 K. The crystal structure corresponding to this relaxed state shows significant decreases of the Fe−N bond distances (Table 2) with an averaged value of 2.018(3) Å. From this, the corresponding HS residual fraction may be roughly estimated as about 25%. This confirms the incomplete nature of the HS/LS thermal conversion deduced from the magnetic data. When a single crystal is subsequently irradiated at 10 K, the average Fe−N distance increases to 2.156(3) Å, very close to the corresponding value observed at room temperature [2.159(2) Å], the trigonal distortion parameters are also quite comparable. This behavior is a clear structural signature that an LS-to-HS quantitative photoinduced process occurs in **1**, in agreement with the photomagnetic properties. The general trend followed by the trigonal distortion underlines the fact that the LS/HS transition is always accompanied by an O_h to D_{3h} trigonal deformation.

The evolution of the intrachain and interchain Fe···Fe separation distance parallels the evolution of the cell parameters because the chains are aligned along the crystallographic *a* axis. Accordingly, the intrachain Fe···Fe distance decreases by only ca. 2.3% from room temperature to the 10 K relaxed state [from 11.3762(3) to

(59) Decoster, M.; Conan, F.; Kubicki, M.; Le Mest, Y.; Richard, P.; Sala-Pala, J.; Toupet, L. *J. Chem. Soc., Perkin Trans. 2* **1997**, 265–271.

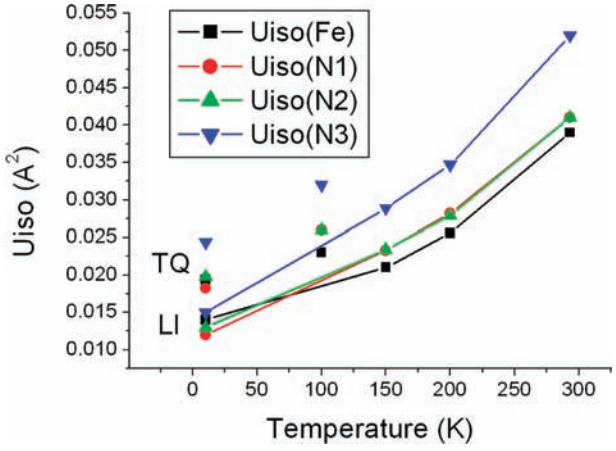

Figure 9. Evolution of the equivalent isotropic atomic displacement factor U_{iso}. LI and TQ denote the 10K light-induced and 10 K thermally quenched states, respectively. The line is only a guide for the eye and joins the 298−200−150 K LI values; it corresponds approximately to the decrease in the thermal vibration of the HS state.

11.1139(2) Å] under the combined influence of the incomplete SCO and thermal contraction. It is to be noted that the 10 K light-induced state and the room temperature state exhibit very similar Fe···Fe distances [11.3894(8) and 11.3762(3) Å, respectively]. On the contrary, the interchain distances mostly depend on the thermal contraction effects with ca. 8.59, 8.47, and 8.50 Å for the room temperature, 10 K light-induced, and 10 K relaxed states, respectively.

Evolution of the equivalent isotropic displacement parameters of the coordinating N atoms (N1, N2, and N3) is very informative (Figure 9). The atomic displacement parameters follow a general decreasing trend for the 298−200−150−10 K light-induced states, as is expected for a decrease of the vibration amplitudes as the temperature is reduced.

These four temperatures are highly relevant because, according to the magnetic data, they correspond to a very large majority of HS species, and therefore the corresponding crystal structures are only marginally biased by the presence of a minority of LS species. The displacement amplitudes corresponding to the 100 K and thermally quenched states are obviously much higher than expected from this general trend. This is attributed to the additional static contribution to the displacement parameters originating from the superposition of HS and LS structural configurations on the same crystallographic position. This behavior is not unusual and has already been reported for related two-step SCO materials with only one Fe^{II} site and for which no ordered superstructure with alternating HS/LS long-range arrangement has been evidenced in the intermediate phase.[70,71]

These structural modifications with temperature and upon irradiation have been completed by the temperature dependence of the unit cell volume (Figure 10). Upon an increase in the temperature from the light-induced state at 10 K, the unit cell volume is almost constant until ca. 35 K, at which a drastic decrease of the volume is observed (from nearly 1629 to 1618 $Å^3$), owing to the HS-to-LS relaxation.

This study suggests that at around 35 K the photoinduced HS state is no longer observable and relaxes to the LS state; this value is comparable to the T(LIESST)

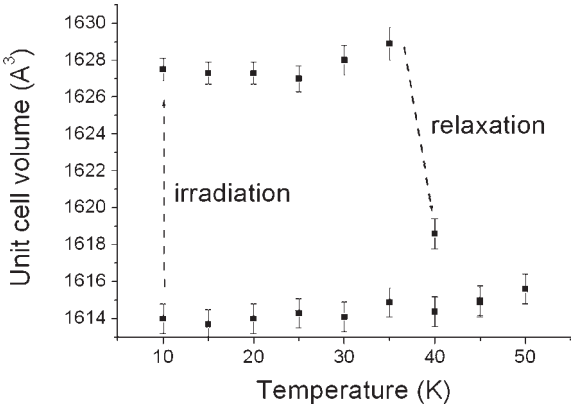

Figure 10. Evolution of the unit cell volume of **1** under irradiation and after relaxation.

value derived from the photomagnetic data. The unit cell volume of the thermally quenched state is intermediate between those of the light-induced and relaxed states.

Discussion

The characteristics of the spin transition in the title compound, namely, a gradual two-step transition in a 1D polymeric compound, raise two fundamental questions: (i) what is the microscopic origin for the two-step character and (ii) what is the reason for the residual HS fraction at low temperature.

Two-step transitions have been reported for a number of SCO materials with various structural architectures, mononuclear or dinuclear discrete entities, as well as polymeric systems. Within the families of mononuclear and dinuclear compounds, the origin of the two-step transition has been most often traced back to the presence of two (or more) crystallographically inequivalent Fe^{II} sites in the unit cell that undergo their respective spin transitions at two different temperatures[60−62] or more seldom to the development of a superstructure intermediate phase resulting from a structural phase transition (symmetry breaking) and long-range ordering; this intermediate phase is thermodynamically stable over a restricted temperature range.[63−67] The latter case is clearly identified from the presence of superlattice reflections on the diffraction pattern and/or by a space group change of the crystal structure. However, in some instances, only one crystallographic Fe^{II} site may be identified for mononuclear materials; the resulting crystal structure of the intermediate phase exhibits structural parameters (e.g., ⟨Fe−N⟩)

(60) Klingele, J.; Kaase, D.; Klingele, M.; Lach, J.; Demeshko, S. *Dalton Trans*. **2010**, *39*, 1689.
(61) Yamada, M.; Ooidemizu, M.; Ikuta, Y.; Osa, S.; Matsumoto, N.; Iijima, S.; Kojima, M.; Dahan, F.; Tuchagues, J.-P. *Inorg. Chem*. **2003**, *42*, 8406–8416.
(62) Amoore, J. J. M.; Kepert, C. J.; Cashion, J. D.; Moubaraki, B.; Neville, S. M.; Murray, K. S. *Chem.—Eur. J*. **2006**, *12*, 8220–8227.
(63) Bréfuel, N.; Watanabe, H.; Toupet, L.; Come, J.; Matsumoto, N.; Collet, E.; Tanaka, K.; Tuchagues, J.-P. *Angew. Chem., Int. Ed*. **2009**, *48*, 1475–1479.
(64) Boinnard, D.; Bousseksou, A.; Dworkin, A.; Savariault, J.-M.; Varret, F.; Tuchagues, J.-P. *Inorg. Chem*. **1994**, *33*, 271–281.
(65) Chernyshov, D.; Hostettler, M.; Törnroos, K. W.; Bürgi, H.-B. *Angew. Chem., Int. Ed*. **2003**, *42*, 3825–3830.
(66) Bonnet, S.; Siegler, M. A.; Costa, J. S.; Molnar, G.; Bousseksou, A.; Spek, A. L.; Gamez, P.; Reedijk, J. *Chem. Commun*. **2008**, 5619–5621.
(67) Nakano, K.; Kawata, S.; Yoneda, K.; Fuyuhiro, A.; Yagi, T.; Nasu, S.; Moritomo, S.; Kaizaki, S. *Chem. Commun*. **2004**, 2892–2893.

intermediate between the HS and LS values, thus indicative of a statistically disordered mixture of HS and LS species.[68] A similar situation has even been reported for a dinuclear system with all Fe^{II} sites presenting statistical HS/LS disorder.[69] Reported two-step transitions in polymeric SCO materials are still rather scarce. Except for the obvious cases of several independent Fe^{II} sites, three examples exhibit a two-step transition corresponding to a single crystallographic site.[45,70,71] In these three examples, a complete HS/LS disorder has been structurally characterized for the intermediate phase and no space group change has been observed during the spin transition. However, in one case, the presence of diffuse scattering clearly evidences a short-range ordering.[45] A number of theoretical models that can explain the occurrence of two-step spin transitions have been proposed.[66,72−79] The first series of models[72−76] relies on a two-coupled-sublattice hypothesis and may be easily pictured as the cases with two independent Fe^{II} sites. The second series of models[77,78] rather considers the interplay between negative (antiferromagnetic-like) short-range and positive (ferromagnetic-like) long-range interactions. Under certain conditions, some of these models may lead to ordered superstructures. Specifically, the axial next-nearest-neighbor Ising-like model (ANNNI model),[72] with competing antiferromagnetic-like first-neighbor and ferromagnetic-like second-neighbor interactions, leads to an intermediate-ordered HS−LS−HS−LS infinite 1D superstructure.[45]

According to all of our experimental findings, several hypotheses may be formulated that could explain the occurrence of two-step character in $[Fe(abpt)_2(tcpd)]$. The derived crystal structures in all of the intermediate situations (100 K, 10 K relaxed, and 10 K flash-cooled) indicate that the asymmetric unit contains only one crystallographic Fe^{II} site, albeit with a $\langle Fe-N \rangle$ value intermediate between a pure HS and a pure LS value. The crystallographic Fe^{II} site is occupied by a statistical spatial distribution of HS and LS species. Neither superstructure reflections nor diffuse scattering have been clearly detected on the measured diffraction patterns. Accordingly, we can reject a hypothesis of long-range HS−LS−HS−LS 1D ordering for the intermediate phase, such as those evidenced for $[Fe(NCSe)_2(bdpp)]$.[45] The two-step transition may simply originate from the presence of two differing Fe^{II} environments (as depicted Figure 2b) statistically distributed along the 1D chains, leading to two distinct Fe^{II} sites with different effective ligand fields. This hypothesis is unlikely according to our crystallographic findings and may be ruled out. Indeed, we managed to efficiently separate the two contributions to the structural disorder of the bridging $(tcpd)^{2-}$ anion. This structural treatment leads to a unique position of the N3 atom, common to both orientations of the bridging ligand. As a consequence, the obtained coordination geometry for the two possible Fe^{II} sites is similar.

On the contrary, a possible local ordering may be pictured as ordered 1D HS−LS−HS fragments of limited length that are statistically distributed along the 1D chain. This is intrinsically the same explanation as that invoked for $[Fe(NCSe)_2(bdpp)]$ but with a reduced correlation length of the ordering. This results most probably from the presence of two closely related environments for the Fe^{II} ions appearing upon lowering the temperature, during the SCO transition. Thus, when the temperature is lowered below ca. 170 K, the SCO transition taking place at one Fe^{II} ion implies the shortening of the Fe−N bond distances (including the Fe−N3 distance), resulting in a slight shift of the corresponding bridging $(tcpd)^{2-}$ ligand. This movement of the ligand produces a lengthening of the Fe−N3 bond distance at the other end of the $(tcpd)^{2-}$ bridges. This longer Fe−N3 bond distance implies a weaker ligand-field strength, leading to a lower transition temperature, in agreement with the experimental finding. This process leads to antiferromagnetic-like first-neighbor interactions (in the ANNNI model) between neighboring sites transmitted along the 1D chain through the $(tcpd)^{2-}$ bridge. A similar explanation also holds for the SCO transitions, where two-step SCO transitions are also observed, such as in the chain compound $[Fe(NCSe)_2(bdpp)]$[43,44] or dinuclear SCO entities[45,80,81] with quite rigid bridging ligands (such as $[Fe_2(PMAT)_2]$ or $[Fe_2(ddpp)_2(NCS)_2]$, for instance). In the latter cases, the spin transition occurring at one of the two Fe^{II} sites perturbs enough the coordination geometry of the second Fe^{II} site to modify significantly its ligand-field energy. As a consequence, the transition temperature of the second Fe^{II} site may be shifted, leading to a two-step transition; this may even suppress any second transition; the material exhibits an incomplete SCO behavior. In the case of compound **1**, the situation is much more complicated because its overall structure is formed by chains presenting two statistically different orientations of the $(tcpd)^{2-}$ ligand (see Figure 2). This fact implies that the SCO transition may be viewed as a multistep process operating statistically along the molecular chain. A clear structural signature of such a process is the abnormally enlarged vibration ellipsoids of the atoms of the $(tcpd)^{2-}$ ligand and the correlatively abnormally high U_{iso} values as discussed above, or at least the most sensitive N3 atom. We have no definite clues of the length of the proposed 1D HS−LS−HS fragments in the intermediate phase; the absence of any noticeable diffuse scattering using our laboratory diffraction equipment indicates that this HS−LS−HS ordered arrangement, if any, is of very restricted length.

(68) Matouzenko, G.; Luneau, D.; Molnar, G.; Ould-Moussa, N.; Zein, S.; Borshch, S. A.; Bousseksou, A.; Averseng, F. *Eur. J. Inorg. Chem.* **2006**, 2671–2682.
(69) Ortega-Villar, N.; Thompson, A. L.; Munoz, M. C.; Ugalde-Saldivar, V. M.; Goeta, A. E.; Moreno-Esparza, R.; Real, J. A. *Chem.—Eur. J.* **2005**, *11*, 5721–5734.
(70) Rodriguez-Velamazan, J. A.; Castro, M.; Palacio, E.; Burriel, R.; Kitazawa, T.; Kawasaki., T. *J. Phys. Chem. B* **2007**, *111*, 1256–1263.
(71) Grunert, C. M.; Schweifer, J.; Weinberger, P.; Linert, W.; Mereiter, K.; Hilscher, G.; Muller, M.; Wiesner, G.; van Koningsbruggen, P. J. *Inorg. Chem.* **2004**, *43*, 155–165.
(72) Boukheddaden, K.; Linares, J.; Tanasa, R.; Chong, C. *J. Phys.: Condens. Matter* **2007**, *19*, 106201.
(73) Bousseksou, A.; Nasser, J.; Linares, J.; Boukheddaden, K.; Varret, F. *J. Phys. I* **1992**, *2*, 1381–1403.
(74) Boukheddaden, K.; Linares, J.; Codjovi, E.; Varret, F.; Niel, V.; Real, J. A. *J. Appl. Phys.* **2003**, *93*, 7103.
(75) Luty, T.; Yonemitsu., K. *J. Phys. Soc. Jpn.* **2004**, *73*, 1237.
(76) Sasaki, N.; Kambara, T. *Phys. Rev. B* **1989**, *40*, 2442.
(77) Romstedt, H.; Hauser, A.; Spiering, H.; Gütlich, P. *J. Phys. Chem. Solids* **1998**, *59*, 1353.
(78) Chernyshov, D.; Bürgi, H.-B.; Hostettler, M.; Törnroos., K. W. *Phys. Rev. B* **2004**, *70*, 094116.
(79) Bolvin, H. *Chem. Phys.* **1996**, *211*, 101–114.
(80) Klingele, M. H.; Moubaraki, B.; Cashion, J. D.; Murray, K. S.; Brooker, S. *Chem. Commun.* **2005**, 987.
(81) Amoore, J. J. M.; Kepert, C. J.; Cashion, J. D.; Moubaraki, B.; Neville, S. M.; Murray, K. S. *Chem.—Eur. J.* **2006**, *12*, 8220.

The presence of residual HS species below the thermal transition is by far not uncommon in SCO materials. It may quite often result from crystal defects, impurities, or structural disorder, as well as kinetic trapping. For compound **1**, we consider that the chain structural distortion process discussed above induces a modification of the ligand-field splitting of the still unconverted HS species while HS Fe^{II} ions are progressively switched to the LS state, leading to a trapping of ca. 25% HS species. Additional evidence for this is observation of the reverse-LIESST process at very low temperature because, by irradiation using a diode laser at 830 nm, an almost complete HS/LS spin conversion occurs. In fact, at low temperature the influence of the entropy (which is the driving force of the SCO phenomenon) becomes minorless with regard to the enthalpy, and as a consequence for a material presenting a gradual spin transition occurring at low temperature, some of the iron(II) metal centers may remain HS whatever the temperature. Interestingly, up to now, in all of the examples where the photomagnetic properties have been carefully investigated,[82,83] it has been observed that the change in the slope of the thermal SCO transition (which defined the almost final residual HS fraction) occurs at the crossing vicinity of the T(LIESST) region (see Figure 5, arrow symbol). The T(LIESST) limit represents, in fact, the region where the lifetime of the photoinduced HS state is very long because of the existence of an activated barrier that slows the relaxation process. In the present work, we evidenced for the first time that this peculiar situation also corresponds to the crossing of the reverse-LIESST effect (see Figure 5, arrow symbol).

Conclusions

In summary, we have reported here the synthesis and crystallographic and photomagnetic properties of both thermal-induced and photoinduced HS states of the first SCO iron(II) molecular neutral chain [$Fe(abpt)_2(tcpd)$] (**1**). The molecular chain structure of **1** is generated by the $(tcpd)^{2-}$ anion acting as a μ_2-bridging ligand via two N atoms of two different $-C(CN)_2$ wings with a statistical disorder in the organic anion, leading to two different orientations of the ligand and to an overall chain structure with two kinds of Fe−anion−Fe bridges statistically distributed along the infinite chain. This description is clearly supported by the crystallographic data because all attempts to solve the crystal structure in lower symmetry (monoclinic or triclinic noncentrosymmetric space groups), to detect whether the two orientations of the organic ligand are ordered, led us to the statistical disorder showing the same orientations. X-ray diffraction studies at low temperature (293−10 K) show a strong modification of the iron coordination, in agreement with the presence of a SCO transition in **1**. Upon irradiation at 10 K, the average Fe−N bond distance and the octahedral distortion parameters recover the room temperature value [2.156(3) Å], indicative of a quantitative light-induced SCO transition. After relaxation, these structural features indicate that ca. 25% of the iron centers remain in the HS configuration at low temperature. In the same temperature range, the unit cell volume variation suggests a T(LIESST) value of ca. 35 K. These observations are in good agreement with the magnetic data because the thermal variation of the $\chi_m T$ product shows an incomplete gradual SCO transition (between 170 and 50 K) with two inflection points at 105 and 60 K. Below 50 K, the magnetic behavior shows a residual HS fraction of ca. 25%, as expected from the crystal data at 10 K after relaxation. The presence of the two inflection points and the residual HS fraction may be explained by the chain structural distortion as the thermal spin transition proceeds, combined with disorder effects. Irradiation of **1** at 10 K shows a gradual increase of the magnetic moment that vanishes as the temperature is increased with an inflection point at ca. 35 K [T(LIESST)] similar to that observed in the photocrystallographic experiments. Therefore, the structural and magnetic data confirm the presence of SCO and LIESST effects in the chain compound [$Fe(abpt)_2(tcpd)$]. Interestingly, this compound also presents a reverse-LIESST effect by using a diode laser at 830 nm, leading to an almost complete HS/LS spin conversion, leaving only ca. 15% of the HS fraction.

From the synthetic point of view, this study confirms the ability of the polynitrile anions to act as bridging ligands to generate new SCO complexes exhibiting original extended arrangements. A further advantage of these anions comes from their ability to be reduced or oxidized to generate polynitrile radical anions that, besides their high capacity to coordinate and bridge transition-metal ions, can transmit the magnetic coupling between them in a much more effective way.[59] Attempts to prepare multidimensional magnetic architectures or metal complexes combining SCO behavior and magnetic interactions using such "radical ligands" are underway.

Acknowledgment. The authors acknowledge the CNRS for PICS project, Brest and Nancy Universities, the Ministère de la Recherche (PPF "Cristallographie et Photocristallographie à haute résolution"), the European Union (COST Action D35-WG-0010-05/0011-05 and MAGMANet network of excellence), the Spanish Ministerio de Educación y Ciencia (Projects MAT2007-61584 and CSD 2007-00010 Consolider-Ingenio in Molecular Nanoscience), and the Generalitat Valenciana (Project PROMETEO 2009/095) for financial support.

Supporting Information Available: X-ray crystallographic data in CIF format. This material is available free of charge via the Internet at http://pubs.acs.org. CCDC reference numbers for **1**: 705802 (293 K), 775315 (200 K), 775314 (150 K), 705803 (100 K), 705804 (10 K flash cooled), 705805 (10 K light induced), and 751547 (10 K relaxed state). These have been deposited with the Cambridge Crystallographic Data Centre and can be obtained, upon request, from the Director, Cambridge Crystallographic Data Centre, 12 Union Road, Cambridge CB2 1EZ, U.K.

Note Added after ASAP Publication. This paper was published ASAP on September 17, 2010, with errors in the author affiliations and minor text errors throughout. The corrected version was reposted on September 22, 2010.

(82) Balde, C.; Desplanches, C.; Gütlich, P.; Freysz, E.; Létard, J.-F. *Inorg. Chim. Acta* **2008**, *361*, 3529–3533.
(83) Neville, S. M.; Etrillard, C.; Asthana, S.; Létard, J.-F. *Eur. J. Inorg. Chem.* **2010**, 282–288.